Optical system for the measurement of the surface topography of additively manufactured parts

Narcís Vilar[1], Roger Artigas[1], Carlos Bermudez[1], Adam Thompson[2], Lewis Newton[2], Richard Leach[2], Martí Duocastella[3], Guillem Carles[1]

[1]Sensofar Tech S.L., Parc Audiovisual de Catalunya, BV-1274 km 1, 08225 Terrassa, Spain.
[2]Advanced Manufacturing Building, Jubilee Campus, University of Nottingham, Nottingham NG8 1BB, UK.
[3]Department of Applied Physics, University of Barcelona, C/Martí i Franquès 1, 08028 Barcelona, Spain.

E-mail: `vilar@sensofar.com`

18 July 2022

Abstract. Additive manufacturing is now regularly used for customised fabrication of parts with complex shapes and geometries. However, the large range of relevant scales, high slopes, step-like transitions, undercuts, alternation between dark and overly bright regions and other complex features present on the surfaces, in particular of metal additive parts, represent a significant challenge for current optical measurement technologies. Measuring surfaces with such complex features requires high numerical aperture optics, and state-of-the-art systems commonly include optics that can only reliably acquire surface topographies over a small field of view, typically tens or hundreds of micrometers. Such measurements are often insufficient for practical applications. Here, we present an optical system that features a large numerical aperture (>0.3) and a wide field of view (2.9×2.9) mm, capable of measuring additive manufacturing parts in a single measurement, without the need for lateral stitching to increase the field of view. The proposed system exhibits optical properties that provide facility for large-field, high-resolution measurement of industrially-produced additively manufactured parts.

Keywords: Additive Manufacturing, Optical metrology, field of view, numerical aperture
Submitted to: *Metrology for Additive Manufacturing*

1. Introduction

The capability of additive manufacturing (AM) technologies for on-demand fabrication of customized parts renders them ideal for prototyping and creating geometries that are too complex, or even impossible to manufacture using traditional methods [1]. Unfortunately, the parts fabricated using AM processes can be difficult to measure and characterise using traditional measurement tools [2, 3]. Specifically, the surfaces of metal AM parts feature a large range of relevant scales, high local slopes, step-like transitions, undercuts, alternation between dark and overly bright regions and other complex features that result from the manufacturing process [4, 5]. These properties are particularly problematic for optical measurement technologies [6], which offer rapid areal measurements but can result in high levels of measurement error when employed for the measurement of irregular surfaces: high local slopes can reflect light at angles that exceed the numerical aperture (NA) limitation of the optical system, which can cause erroneous and non-measured points (NMP). This problem is typically addressed by using a higher NA objective. However, higher NA optics often feature smaller fields of view (FOV), and are not capable of capturing the larger, lower spatial-frequency components of the topography. The common solution to this issue is to increase the measurement area by lateral scanning and stitching of individual FOVs, but the associated increase in acquisition time and induced errors may be unacceptable. An optical system with sufficient NA and FOV would allow for measurement of metal AM parts with sufficient resolution and speed, without the need for stitching. However, the design of such an optical system is complex: to achieve high NA and wide FOV simultaneously there is a need to employ large optical apertures, which increases the difficulty in controlling optical aberrations.

Optical techniques have proven to be advantageous over tactile profilometry to characterise surfaces in AM, such as confocal microscopy [6] or coherence scanning interferometry [7], highlighting the importance of high-dynamic range and NA. This was also supported with multi-scale analysis [8], indicating that optical techniques are better suited at micrometer scales than coordinate measuring machines or tactile profilometry for measuring metal AM surfaces. Within the most common optical methods, focus variation techniques are shown to be highly robust for measuring for AM parts although with somewhat lower lateral and vertical resolutions [9]. The combination of confocal and focus variation data has been suggested and proven to reduce the quantity of NMP [10]. Optical methods have been compared for performance, concluding that measurement discrepancies occur due to high local slopes and high aspect ratios of the surface features, which result in measurement artefacts [11]. Focus variation provides the fastest measurements although with a lower spatial resolution. Coherence scanning interferometry provides the best resolution and with virtually no measurement artefacts, but requires a longer measurement time and is least robust against vibrations. Confocal lays between focus variation and coherence scanning interferometry, which makes it a good choice for fast measurements of high-resolution topographies, although issues such as the quantity of NMP and measurement artefacts need to be addressed.

Here, we report the design, assembly, characterisation, and experimental results of an optical system for AM (OSAM) surface measurement. By adapting a commercial stereo-microscope objective, OSAM is capable of measuring the surface topography of metal AM parts over large areas with sufficient resolution. We provide an in-depth characterisation of the optical properties of the system and demonstrate its potential for AM surfaces by measuring a variety of test objects.

2. Optical design

The key component in achieving the required combination of high NA and large FOV is the objective lens. Among the commercially available objectives, those designed for stereo microscopes provide relatively high apertures for a given magnification (and so FOV for a given camera sensor). The proposed solution follows from the selection of a commercially available objective and the design of a dedicated tube lens. We used a Nikon SHR Plan Apo 2×, with a reported NA of 0.312 and a back aperture diameter around 50 mm. The main challenge in adopting this type of objective for surface topography measurement is the design of a tube lens so that it avoids vignetting and minimises aberrations. We designed such a tube lens using ray-tracing software, while adopting an additional constraint: using only commercially available lenses. This restriction adds complexity in terms of selecting optimal materials, curvature and thicknesses from the pool of available lenses, but makes the system simpler to replicate. Our design required a total of five lens elements (two singlets and three doublets). A schema of the design is shown in figure 1. The tube lens has a focal length of 169.7 mm and its performance is close to the diffraction limit over a field up to 6 mm at the image plane, providing a FOV at the sample plane of approximately (2.9×2.9) mm. To achieve such a wide measurement area with a sufficient sampling rate, a large sensor with a high pixel count is required. We used a sensor with (5320×4600) pixels and 2.74 µm pitch (BFS-U3-244S8M-C, FLIR).

OSAM was designed to obtain optical sectioning

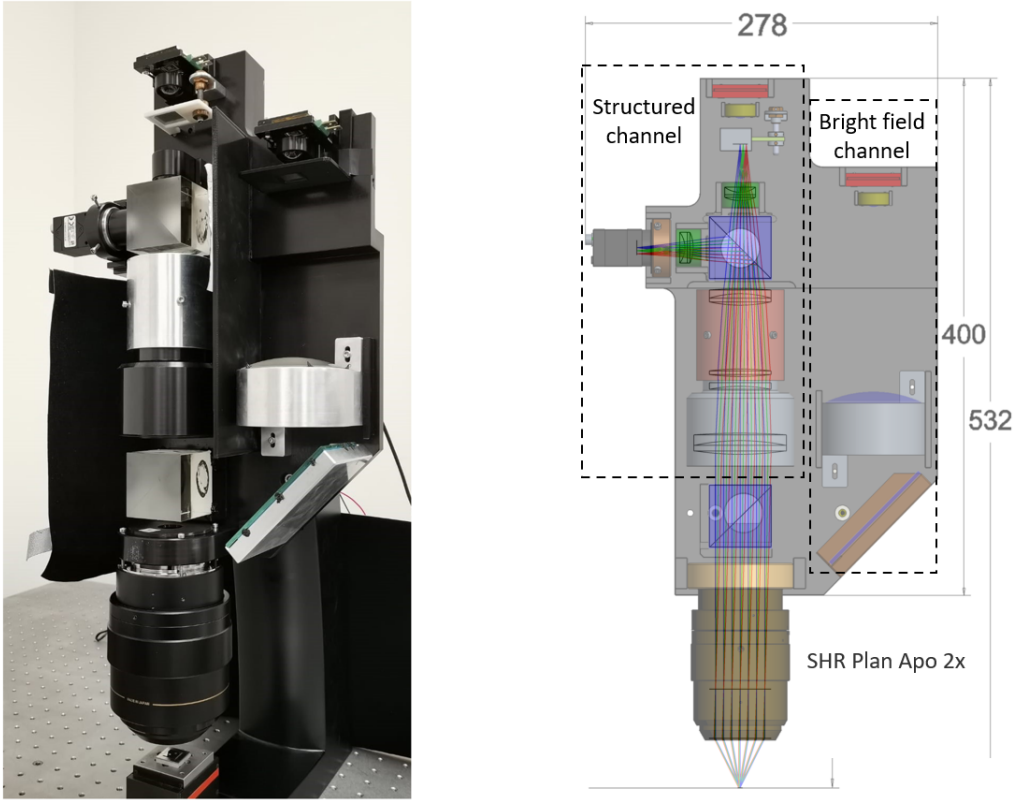

Figure 1: OSAM design: left) picture of the assembled system; and right) corresponding CAD schema. For both illumination channels, LEDs (in red) are used as light sources. The light is directed through condensers (shown in yellow), lenses and finally to the objective. The reflected signal from both paths is collected using the same objective, and acquired with a single camera. Raytraced simulation is included for the structured-illumination and (reflected) imaging paths. All units are in millimeters.

through a confocal technique called "Hi-Lo" [12, 13]. In contrast to traditional confocal microscopy, implemented, for example, with a spatial light modulator [14, 15], Hi-Lo does not require specialised equipment, which reduces the engineering complexity and cost of the instrument. The technique is based on the sequential acquisition of two images: a bright-field image and a structured-illumination image. We designed our system to obtain such images using two different illumination channels.

The imaging path and the two illumination paths are coupled by two beam splitters (see figure 1). The structured illumination path incorporates a mask, made of a periodic structure of transmissive and reflective stripes (a chrome-on-glass Ronchi grating) with a spatial frequency of 20 lp/mm, to create the illumination pattern projected at the sample plane (see figure 1). It should be noted that this path uses the same tube lens as the imaging path, as high-quality imaging performance is required to sharply project the illumination pattern. However, for the bright-field channel, a simpler lens was employed. This architecture enables fast, electronic switching of the illumination LEDs (Luminus CBT-90 Green), which allows for faster axial scanning. Acquisition speed is, in practice, limited by the camera frame rate and processing time.

The images are first combined to obtain the "low" spatial-frequency components of the optical section. This step is performed by subtracting the bright-field image from the structured-illumination image, resulting in a signal that is optically sectioned. Then, the "high" image is obtained by high-pass filtering of the bright-field image, and the high spatial-frequency content is transferred to the optically-sectioned image by combination in the Fourier domain, effectively blending the "high" and "low" images into a sharp optically-sectioned image. By sequentially acquiring optical sections at different axial locations (obtained by displacing the entire system), a topography map can be reconstructed.

As typical metal AM samples present relatively rough surfaces, it is possible to use focus variation to detect the optically-sectioned images [16]. However, the Hi-Lo technique is more robust because it can also be used for smooth surfaces (also found on AM,

specially at fully melted regions), so only Hi-Lo results are presented in this paper.

3. Optical characterisation

The focal length and NA of the microscope objective and tube lens are the main parameters that determine the optical properties of the system. To characterise the focal length of the tube lens, we substituted the objective with a 10×/0.3NA objective (with a known focal length of 20 mm) and measured the resulting magnification by imaging a calibrated ruler (Geller Microanalytical Laboratory Inc, MR-1). Using this method, we measured a focal length of 172 ± 5 mm which is sufficiently close to the nominal value of 169.7 mm from the optical design. We then replaced the objective with a Nikon SHR Plan Apo 2× and repeated the same procedure, obtaining a focal length of the objective of 41 ± 2 mm. The overall magnification of OSAM was therefore calculated to be $4.2 \pm 0.3\,\times$. To estimate the maximum NA of the objective (i.e. when the full aperture is used), we placed a tilted mirror at the sample plane. Increasing the angle of the mirror decreases the number of photons that are gathered by the objective, and consequently, captured by the camera. The angle at which virtually no light is collected was approximately 35°, which corresponds to an NA of 0.57. However, the objective is not corrected to work over such high NA in stereoscopy, and we added an aperture of 20 mm in diameter close to its back focal plane to control the effective NA. This addition reduced the NA to approximately 0.26.

To characterise the optical performance of the imaging system, we first used a United Stated Air Force (USAF) resolution test target, (see figure 2a). The bright-field image of the test target provides a direct measurement of the system resolution. The optical system can clearly resolve all spatial frequencies present in the target, up to the maximum frequency of 645 lp/mm (9th group, third element of the USAF target). For a more in-depth characterisation of the resolution of the system, and to estimate its optical cut-off, we used the slanted edge method [17, 18]. From a single image of a sharp and titled edge (see figure 2b), the modulation transfer function (MTF) can be computed. Results from both the slanted edge method and measured points from the USAF target are shown in figure 2c. For reference, we also included the theoretical diffraction-limited and monochromatic MTF using the estimated NA of 0.26. Experimental results were similar to the theoretical prediction, indicating performance close to the diffraction-limit. The measured cut-off spatial frequency for which the MTF is 0.1 is approximately 615 lp/mm, consistent with the maximum frequency resolvable using the USAF test target.

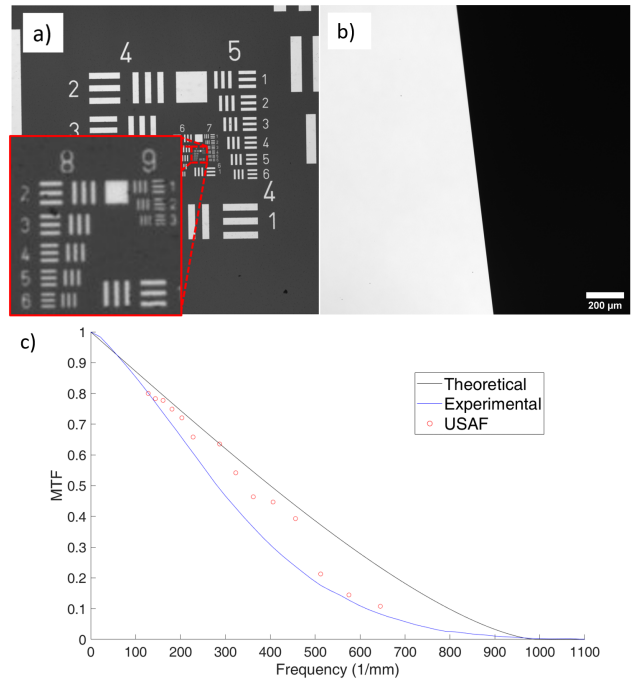

Figure 2: Bright field images acquired with OSAM of: a) United States Air Force (USAF) resolution target; b) Slanted edge; and c) Modulation transfer function obtained with slanted edge method and USAF measurements. The black curve is the theoretical MTF in a diffraction-limited system, the blue curve is the experimental result following the slanted edge method, and circle points represent the calculated contrast values for the highest frequency patterns of the USAF target.

Next, we analysed the performance of the system to retrieve quantitative three-dimensional information from a sample. To this end, we used two certified different material measures: the NPL B40 type AIR material measure [19, 20], and a series of type PGR step height material measure samples (ISO 5436-1) [21]. Results for the NPL B40 type AIR are shown in figure 3, compared with the topography obtained with a commercial confocal system (S neox 090, Sensofar) for reference. A high visual similarity between both measurements can be observed, and for the commercial system it is possible to notice some stitching traces. Texture parameters were calculated from 10 different measurements, and we obtained the values of $Sa = 0.80 \pm 0.04$ µm and $Sq = 1.02 \pm 0.03$ µm for the commercial system, and $Sa = 0.80 \pm 0.04$ µm and $Sq = 1.015 \pm 0.028$ µm for OSAM. Both measurements are consistent with the certified values: $Sa = 0.79 \pm 0.03$ µm and $Sq = 1.01 \pm 0.02$ µm. Importantly, the captured area with the commercial system in figure 3 is the result of stitching nine individual measurement FOVs, while

the same total measurement area was measured with OSAM using a single FOV measurement.

Secondly, we measured a series of type PGR step height material measures samples (ISO 5436-1) [21], each one with a certified height of $7.61 \pm 0.06\,\mu m$, $9.96 \pm 0.07\,\mu m$ and $21.70 \pm 0.02\,\mu m$. Measurements obtained using OSAM are $7.62 \pm 0.06\,\mu m$, $10.15 \pm 0.10\,\mu m$ and $22.04 \pm 0.07\,\mu m$. To illustrate the measurement process (ISO 5436-1 A1), the measurement profile of one step is shown in Figure 4.

All values above include type A expanded uncertainty, U, calculated using:

$$U = ku_c, \tag{1}$$

where u_c is the combined uncertainty, k is the coverage factor for a 95% confidence interval. The combined uncertainty for the measurements of both the NPL B40 type AIR and the PGR step height material measures included the certified and measured uncertainties.

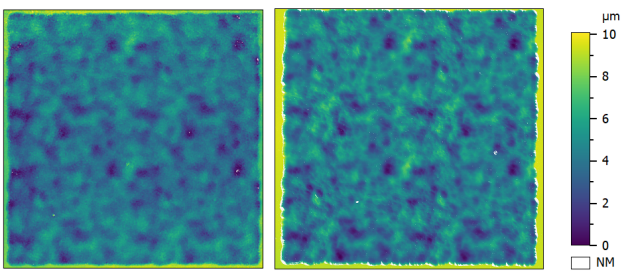

Figure 3: Topography measurements of the NPL B40 Type AIR using: right) the commercial confocal system S neox 090, with texture parameters $Sa = 0.80 \pm 0.04\,\mu m$ and $Sq = 1.02 \pm 0.03\,\mu m$; left) OSAM, with texture parameters $Sa = 0.80 \pm 0.04\,\mu m$ and $Sq = 1.015 \pm 0.028\,\mu m$. The certified area measures (1.5×1.5) mm and the topography obtained with the commercial system is the result of stitching of nine individual measurement FOVs.

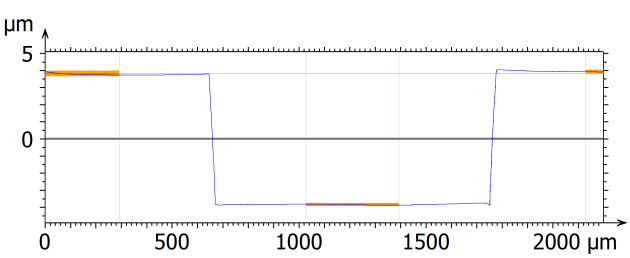

Figure 4: Plot of the profile of the step sample measured according to ISO 5436-1 A1. The obtained value is $7.62 \pm 0.06\,\mu m$.

Finally, we quantified three key ISO 25178-600 [22] metrological characteristics for assessing the performance of an areal measurement system: the flatness deviation, instrument noise and z-axis amplification coefficient, α_z [23, 24]. For the flatness deviation and instrument noise we obtained $Sz = 67 \pm 20\,nm$ and $Sq = 62 \pm 3\,nm$, respectively. For determining the z-axis amplification coefficient we used the measurements of the step heights mentioned above, which resulted in $\alpha_z = 0.992$. All uncertainties are type A expanded and were obtained from 10 different measurements.

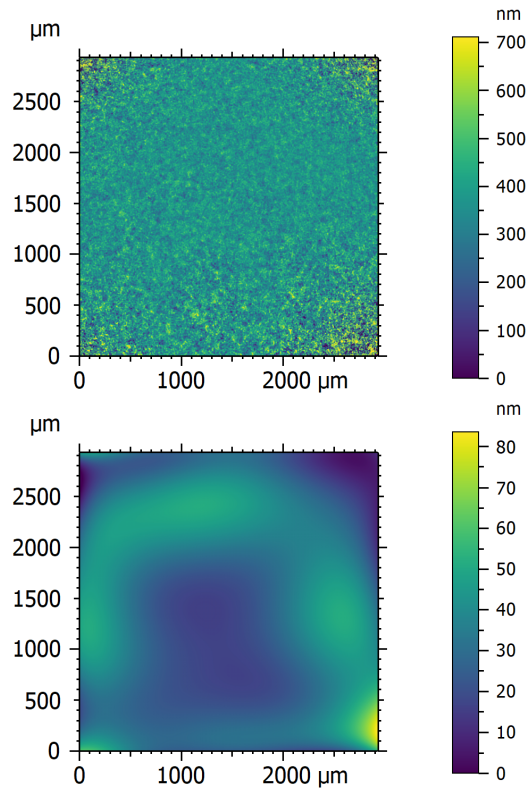

Figure 5: One of the measurements of: top) system noise measured according to ISO 25178-600; and bottom) flatness deviation.

4. Results and discussion

To demonstrate the suitability of OSAM for measuring AM parts, we acquired topography images of a prototype 3D roughness artefact (3DRS) (similar to that reported in [25]). This measurement artefact was manufactured using AM techniques and has four different faces (denoted I, II, III, IV) that aim to be illustrative of a range of common surface finishes from various metal AM processes (see figure 6). Each face is designed to have different surface texture parameters compared to the other surfaces. Faces I and IV of the artefact were rougher than faces II and III.

Initially, we evaluated how the surface texture parameters obtained from measurements using OSAM

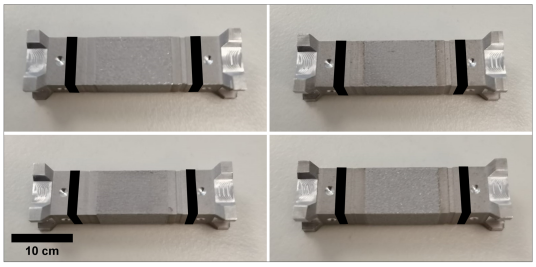

Figure 6: Photographs of each of the faces of the NPL 3DRS. The faces are numerated in roman numerals at each side. The black-masked regions are not functionally relevant to the article.

depend on FOV. As a benchmark, we used the commercial confocal system (S neox 090, Sensofar) with three different objectives of varying NA: 10×/0.30NA, 20×/0.45NA, and 50×/0.8NA. We calculated the mean and expanded type A uncertainty of the surface texture parameter *Sa* as a function of FOV, by performing ten independent measurements of the surface face at ten random different locations with no overlap. In this case, the combined uncertainty only includes the measured uncertainty and each single measurement was not repeated (to assess individual uncertainty at each FOV), because the certified values for the artefact are not available and the aim here is to assess the dependence of surface parameters on FOV. For both systems, we measured these parameters in four different square areas, with side lengths of 0.73 mm, 1.46 mm, 2.2 mm and 2.92 mm, respectively. To achieve these measurement areas, lateral scanning and individual FOV stitching was required with the commercial system for the 10× and 20× objectives –the 50× objective has a considerably smaller native FOV and so we only stitched enough individual FOVs to achieve total measurement areas of side length 1.095 mm. Despite the reduced measurement area, this measurement can be used to provide a reference for high NA measurements. For OSAM, the entire measurement area of side length 2.92 mm was acquired with a single acquisition, and smaller FOVs corresponding to the same side lengths were obtained by cropping the measurement to 1024, 2048, 3072 and 4096 pixels, which allowed for direct comparison. Results are shown in figure 7. For both systems, the mean value of *Sa* remains approximately constant (above a given FOV) with the FOV, whereas the uncertainty decreases. This indicates that the FOV plays a critical role: it must be sufficiently large to capture the lowest spatial-frequency components of the topography that are still functionally relevant. For example, for a small FOV, the measurement could include only a small portion of a high peak or valley, resulting in a local surface measurement that is not representative of the entire surface. This factor explains the large uncertainty of the objective with the smallest FOV (the 50× objective). This effect is illustrated in figure 8, where we present a full topography of face I using a 10× objective and (4 × 4) stitching (a) and two sub-regions with a smaller FOV of side length 0.73 mm (b and c). Given the large local variation in surface texture, the measured values obtained in b) and c) are different by almost a factor of two. These results highlight the need for large measurement areas to provide representative measurements, and overall we observe that, for the specimen considered, a FOV of side length approximately 3 mm is required.

An additional exploration of the characteristics of typical AM surfaces can be performed using area-scale analysis. Such approach focuses on the characteristics of the measured surface at different scales, from the largest features to the finest detail that is measured. Various tools can be employed for this, from simpler spatial-frequency analysis using Fourier transforms or band-pass filtering [26], to more elaborated scale-sensitive fractal analysis [27, 28, 29]. Relevant parameters that can be extracted from such analysis include the fractal dimension, smooth-rough crossover, and the surface complexity. For instance, we calculated these parameters from the topographies of the face I of the 3DRS sample, measured with OSAM and the commercial confocal system. We obtained fractal dimensions of 2.10 and 2.09; smooth-rough crossover of 2104 µm^2 and 1900 µm^2; and finally a fractal complexity of 51.9 and 46.5, respectively.

To obtain representative measurements of metal AM parts with a sufficiently low proportion of NMP, not only do we need a high FOV, but also a high NA to capture enough light reflected from the AM surfaces, which are expected to have high local slopes. We assessed the impact of NA using the quality of the topography images of OSAM and the commercial measurement system. Specifically, we imaged the topography of the 3DRS sample using apertures with different diameters of aperture stop. For OSAM, we used apertures up to 30 mm in diameter and for the commercial measurement system we used a 20×/0.45NA objective, with a back aperture (exit pupil) of around 9 mm. Results for OSAM and the commercial system are shown in figures 9 and 10, respectively. Pixels whose axial response (the optically-sectioned signal across the scan) does not reach a high enough signal-to-noise ratio and a minimum threshold (an empirical value which depends on the type of sample and is user-selected) were deemed NMP shown in white in figures 9 and 10. In both cases, as the aperture diameter decreases, the number of NMP increases.

A quantitative assessment of this effect is presented in figure 11, which shows plots of the number

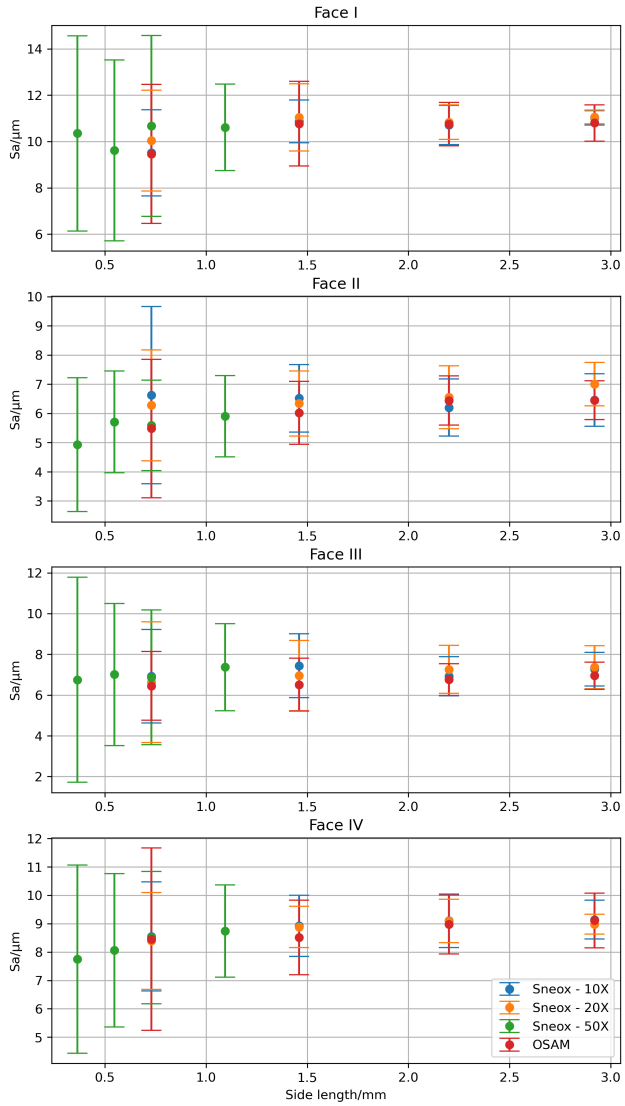

Figure 7: Plots of Sa, error bars represent uncertainty at a 95% confidence interval across 10 different measurements, as a function of FOV. OSAM measurements are compared to those obtained with the commercial confocal system S neox 090 using 10×, 20× and 50× objectives.

of NMP as a function of the aperture size, for OSAM and the commercial system. Plots include results for faces I and II, representative of relatively rougher and smoother surfaces found in common metal AM parts. For the commercial system, two regions can be differentiated. The first region corresponds to NA values below 0.3, which exhibits a strong relationship between the number of NMP and NA; and the second region corresponds to NA values above 0.3, where the number of NMP has a lower variation with NA. This result indicates that most of the sample surface has slopes that can be measured with NA lower than

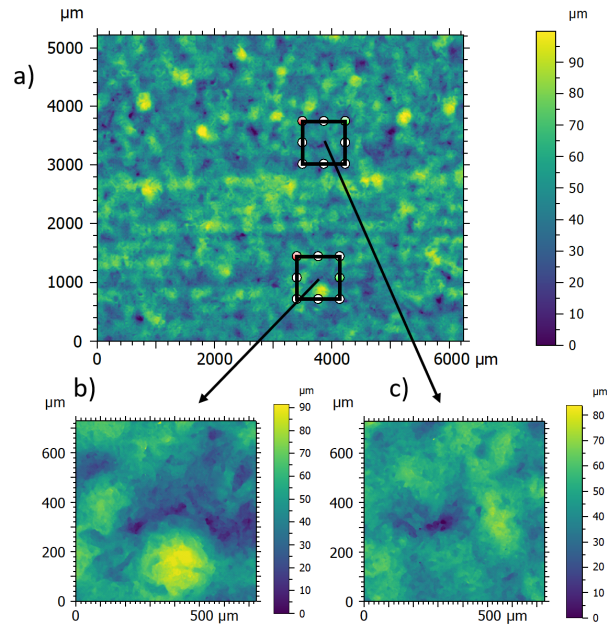

Figure 8: Importance of large measurement areas in measuring AM parts: a) topography image of Face I obtained by stitching (4 × 4) images with the 10× Nikon lens. The black squares represent two regions of interest (ROI); b) topography image of the 1st ROI, with a measured $Sa = 13.069\,\mu m$; and c) topography image of the 2nd ROI, with $Sa = 7.710\,\mu m$. The disparity between measured values makes evident the need for measuring over a large measurement area.

0.3. For NA>0.3, the number of NMP only decreases slightly with NA, that is, only a few additional pixels (7 % approximately in both cases) are measured by further increasing NA. The same trends are observed for the OSAM measurements. It should be noted that, in this case, we plotted the number of NMP against aperture diameter. As can be observed in the lower graph in figure 11, the threshold appears around 15 mm in aperture diameter. In all, these results indicate that, when measuring typical metal AM pieces, an NA of at least 0.3 should be used, which translates to a minimum aperture of 15 mm in our OSAM design.

A low number of NMP has an overall negligible effect on the final measurement since the entire topography can be algorithmically reconstructed correctly using interpolation based on neighbouring pixels. But, when the number of NMPs is high, interpolation fails because NMPs group in large clumps (see figures 9c and 10c). Therefore, the use of a sufficiently high NA is imperative. Unfortunately, conventional objectives with satisfactory NA provide higher magnifications, which comes with a caveat: the loss of FOV and the consequent need for stitching, resulting in increased measuring time and the addition

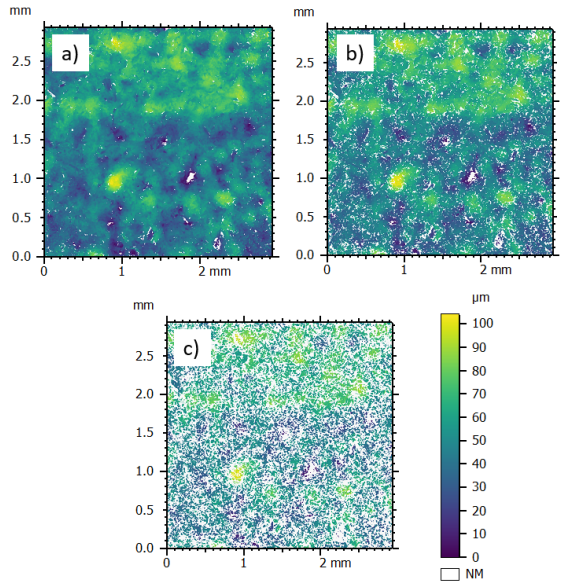

Figure 9: Topography measurements of face I obtained with OSAM using a) 20 mm aperture; b) 14 mm aperture; and c) 12 mm aperture.

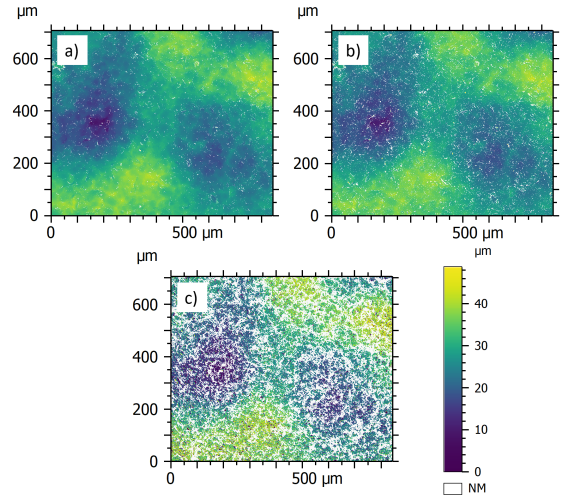

Figure 10: Topography measurements of face II obtained with the commercial optical profiler S neox 090 with a) 9 mm aperture; b) 6 mm aperture; and c) 3 mm aperture.

of stitching errors.

To further illustrate this FOV-against-NA trade-off, and to highlight the benefit provided by OSAM, we measured a flat surface of a specimen manufactured using laser powder bed fusion process on a Renishaw AM250 system (see figure 12). We acquired measurements using the commercial confocal system using a range of objectives (5×/0.15NA, 10×/0.30NA, 20×/0.45NA and 50×/0.8NA) and manually registered the resultant topographies within a single coordinate

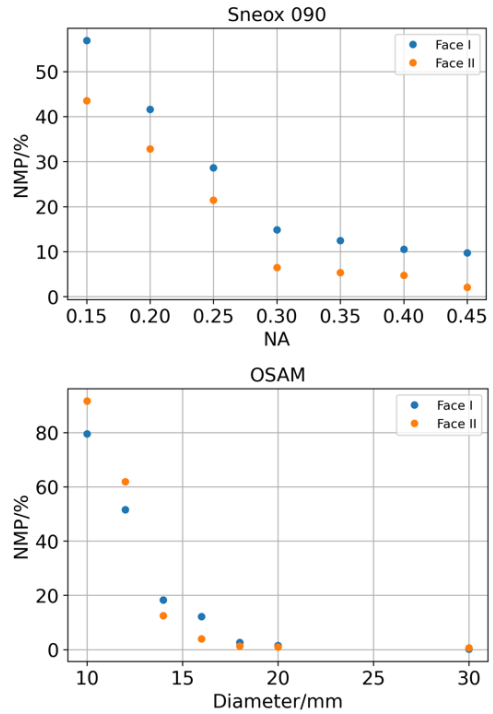

Figure 11: Plot of the percentage of NMPs: top) versus NA, for the commercial optical profiler S neox 090; and bottom) versus aperture stop diameter in OSAM. Face I and II were selected as representative of relatively rougher and smoother surfaces.

system. Measurement results are shown in figure 13 (top), with measured topographies superimposed upon one another. The trade-off between FOV and measurement quality (visually observed through the number of NMP) is evident: the highest NA objectives provide better quality measurements but lose the ability to acquire a statistically significant FOV. We included measurements using the 5×/0.15NA objective as, while the quality of the measurements is clearly deficient, it provides a similar FOV to OSAM. The topography shown in figure 13 (bottom) is obtained using OSAM in approximately the same location. In this case, we have indicated, for reference, the equivalent size of the FOV provided by the commercial system using the different objectives. As can be observed, OSAM can provide surface measurements with a low number of NMP over a relatively wide FOV. The characteristics of the measurement obtained with the commercial system (using each of the objectives) and OSAM are shown in table 1, including the sampling rate at the sample plane and the percentage of NMP when measuring the sample in consideration. OSAM provides a significantly wider FOV (2.92 × 2.92) mm with the lowest proportion of NMP, at around 7 %. Furthermore, the measurement quality

can be observed in figure 14, where we have plotted a horizontal profile extracted from the topographies presented in figure 13, comparing OSAM to the commercial system by employing a range of objective lenses. The low NA objectives are not capable of measuring the surface correctly, producing significant spikes and NMPs, whereas higher NA objectives provide more accurate measurements albeit with the reduced FOV. OSAM data provides a low number of NMP, while covering a relatively large FOV.

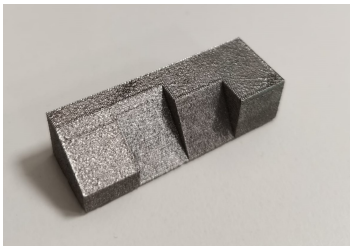

Figure 12: Metal AM specimen. Dimensions are approximately $(40 \times 14 \times 10)$ mm. The top surface (i.e. the final surface parallel to the manufacturing plane) is the surface facing upwards in the image, with other surfaces representing different build angles in the AM system.

Finally, we briefly discuss measurement time. The system presented here is a prototype and was not thoroughly optimised for fast operation, but indicative time landmarks can be drawn for reference. Considering a scanning range sampled at 50 planes, OSAM can provide a measurement with approximately 25 seconds. This time includes acquisition time, per-plane processing time (mainly calculation of the optically-sectioned image), and the topography reconstruction time. The total time is therefore limited by both the camera frame rate, which is limited to 12 frames per second in our case, and the processing power. With further optimisation and use of more powerful processing, we estimate that the OSAM measurement time could potentially be reduced to about 10 seconds, with the current architecture and transfer data rate of the camera. Further reduction would be possible but would require the use of hardware able to operate at unconventionally high data rates. For comparison, the reference confocal system considered is able to provide a 50-plane measurement with approximately 2 seconds. However, fair comparison should consider an equivalent FOV and therefore include the time required for measuring a complete, stitched FOV. The camera of the reference commercial system operates at 60 frames per second with 5 MPx, which ultimately amounts to a similar data rate; sampling the wide FOV provided by OSAM requires a high pixel count, and we use a camera

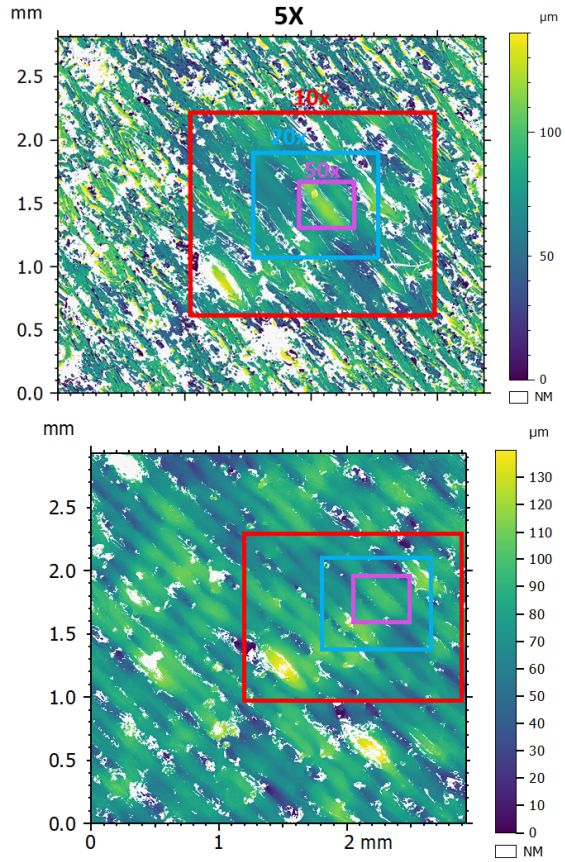

Figure 13: Topography images of the flat surface of metal AM specimen: top) superimposed topographies obtained with objectives 5× (black), 10× (red), 20× (blue) and 50× (violet); and bottom) topography image obtained with OSAM, with the FOV corresponding to the topographies at the top indicated for reference. Qualitatively, OSAM is capable of acquiring accurate topography maps that contain neither spikes nor a high number of NMP.

with 25 MPx limited to 12 frames per second. Of course, stitching has the additional disadvantages of requiring the lateral scanning mechanism, additional time for lateral movement, some degree of FOV overlap for stitching, and potentially resulting in stitching artifacts, which OSAM naturally manages to avoid.

5. Conclusions

The high slopes and surface texture of metal AM parts impose severe optical specifications for surface measurement systems to reliably measure surface topography and obtain representative surface texture parameters. To avoid a significant number of NMP, a NA above 0.3 is desired. Conversely, a minimum measurement area of around (3×3) mm is required,

Objective	NA	FOV		Sampling /(µm/pixel)	NMP/%
		Height/mm	Width/mm		
5×	0.15	2.8	3.3	1.38	32.57
10×	0.30	1.4	1.68	0.69	19.99
20×	0.45	0.7	0.84	0.34	11.48
50×	0.90	0.28	0.34	0.14	9.11
OSAM	0.26	2.92	2.92	0.71	7.02

Table 1: Characteristics for each objective presented in figure 13, including sampling and NMP.

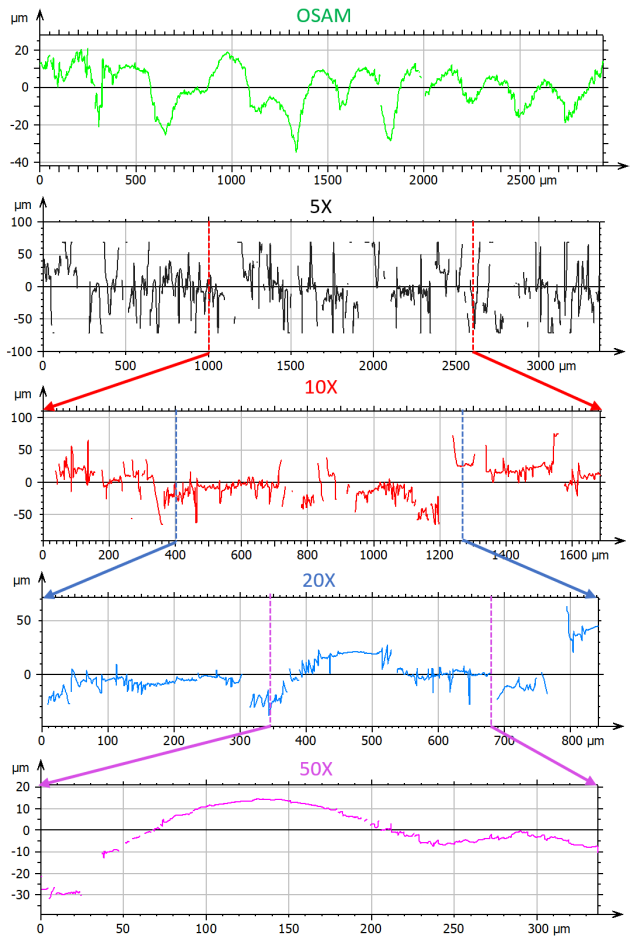

Figure 14: Plot of the profile of the flat surface of metal AM specimen obtained with different objectives: OSAM (green), 5× (black), 10× (red), 20× (blue) and 50× (violet). Although that OSAM's profile is not exactly the same as the commercial system, qualitatively OSAM is capable of obtaining topography maps that do not contain spikes and with a low number of NMP, similar to 20× and 50× objectives but with a much higher FOV.

to capture the highest and lowest relevant spatial frequencies in the topographic oscillations of typical metal AM surfaces. Because no traditional microscope objectives fulfill these characteristics simultaneously, commonly selected objectives are 10×/0.3NA or 20×/0.45NA, which offer a high enough NA, but come with the requirement of stitching several individual FOVs to reconstruct the desired measurement area, which is time-consuming and can result in stitching errors.

As our results demonstrate, high NA but low magnification objectives, such as those available in stereo-microscopy systems, can be adapted for the measurement of AM parts. To this end, we selected an objective, designed a dedicated tube lens, and built OSAM, a complete system capable of reliably measuring surfaces and generating surface texture parameters without stitching. The system implements HiLo confocal microscopy for calculating the surface topography. A benchmark comparison of topographies obtained with a commercial confocal system and OSAM showed no significant differences in generated parameters. We anticipate that such an approach will progressively be adopted as a measurement tool for the rapid and accurate characterisation of AM parts.

6. Acknowledgements

NV, GC and MD would like to thank AGAUR for supporting this project with an Industrial PhD grant DI-2021 19. AT, LN and RKL would like to thank the UKRI Research England Development (RED) Fund for funding their contribution to this work via the Midlands Centre for Data-Driven Metrology.

References

[1] Ngo T D, Kashani A, Imbalzano G, Nguyen K T and Hui D 2018 *Composites Part B: Engineering* **143** 172–196
[2] Townsend A, Senin N, Blunt L, Leach R and Taylor J 2016 *Precision Engineering* **46** 34–47
[3] Leach R, Bourell D, Carmignato S, Donmez A, Senin N and Dewulf W 2019 *Cirp Annals-Manufacturing Technology* **68** 677–700
[4] Senin N, Thompson A and Leach R K 2017 *Measurement Science and Technology* **28** 095003
[5] Senin N, Thompson A and Leach R 2018 *Measurement Science and Technology* **29** 045009
[6] Grimm T, Wiora G and Witt G 2015 *Surface Topography: Metrology and Properties* **3** 014001

[7] Gomez C, Su R, Thompson A, DiSciacca J, Lawes S and Leach R K 2017 *Optical Engineering* **56** 1 – 8

[8] Cabanettes F, Joubert A, Chardon G, Dumas V, Rech J, Grosjean C and Dimkovski Z 2018 *Precision Engineering* **52** 249–265

[9] Newton L, Senin N, Gomez C, Danzl R, Helmli F, Blunt L and Leach R 2019 *Additive Manufacturing* **25** 365–389

[10] Flys O, Berglund J and Rosen B G 2020 *Surface Topography: Metrology and Properties* **8** 024003

[11] Tato W, Blunt L, Llavori I, Aginagalde A, Townsend A and Zabala A 2020 *Procedia CIRP* **87** 403–408

[12] Lim D, Ford T N, Chu K K and Metz J 2011 *Journal of Biomedical Optics* **16** 1–8

[13] Martínez P, Bermudez C, Carles G, Cadevall C, Matilla A, Marine J and Artigas R 2021 Metrological characterization of different methods for recovering the optically sectioned image by means of structured light *Optical Measurement Systems for Industrial Inspection XII* (SPIE) pp 147 – 157

[14] Neil M A A, Juškaitis R and Wilson T 1997 *Optics Letters* **22** 1905–1907

[15] Artigas R, Pinto A and Laguarta F 1999 Three-dimensional micromeasurements on smooth and rough surfaces with a new confocal optical profiler *Optical Measurement Systems for Industrial Inspection* (SPIE) pp 93 – 104

[16] Bermudez C, Martinez P, Cadevall C and Artigas R 2019 Active illumination focus variation *Optical Measurement Systems for Industrial Inspection XI* vol 11056 (SPIE) pp 213 – 223

[17] Burns P 2000 Slanted-edge mtf for digital camera and scanner analysis *Society for Imaging Science and Technology: Image Processing, Image Quality, Image Capture, Systems Conference*

[18] Xie X, Fan H, Wang A, Zou N and Zhang Y 2018 *Appl. Opt.* **57** 6552–6558

[19] Leach R, Giusca C, Rickens K, Riemer O and Rubert P 2014 *Surface Topography: Metrology and Properties* **2** 025002

[20] ISO 25178-70:2014 *Geometrical product specification (GPS) - Surface texture: Areal - Part 70: Material measures* (Vernier, Geneva, Switzerland: International Organization for Standardization)

[21] ISO 5436-1:2000 *Geometrical product specification (GPS) - Surface texture: Profile method; Measurement standards - Part 1: Material measures* (Vernier, Geneva, Switzerland: International Organization for Standardization)

[22] ISO 25178-600:2010 *Geometrical product specification (GPS) - Surface texture: Areal - Part 600: Metrological characteristics for areal-topography measuring methods* (Vernier, Geneva, Switzerland: International Organization for Standardization)

[23] Haitjema H and Leach R 2018 *Surface Texture Metrological Characteristics* (Berlin, Heidelberg: Springer Berlin Heidelberg) pp 1–5 ISBN 978-3-642-35950-7

[24] Giusca C L and Leach R K *Good Practice Guide No.129 Calibration of the metrological characteristics of areal contact stylus instruments* (Teddington, Middlesex, United Kingdom: National Physics Laboratory)

[25] Jones C W, Sun W, Boulter H and Brown B 2022 *Meas. Sci. Technol.* **In press**

[26] ISO 4287:1997 *Geometrical product specification (GPS) - Surface texture: Areal - Surface texture: Profile method — Terms, definitions and surface texture parameters* (Vernier, Geneva, Switzerland: International Organization for Standardization)

[27] Brown C A 2013 *Areal Fractal Methods* (Berlin, Heidelberg: Springer Berlin Heidelberg) pp 129–153

[28] ISO 25178-2:2012 *Geometrical product specification (GPS) - Surface texture: Areal - Part 2: Terms, definitions and surface texture parameters* (Vernier, Geneva, Switzerland: International Organization for Standardization)

[29] ASME B46-1 (2019) *Surface Texture (Surface Roughness, Waviness, and Lay)* (New York, USA: American society of Mechanical engineers)